

**EFFECT OF ELECTRO-CARBURISATION
PROCESS ON THE TRIBOLOGICAL
BEHAVIOR OF MILD STEEL**

JESTER LING LIH JIE



**THIS IS SUBMITTED IN FULFILLMENT FOR
THE DEGREE OF DOCTOR OF PHILOSOPHY**

PERPUSTAKAAN
UNIVERSITI MALAYSIA SABAH

**FACULTY OF ENGINEERING
UNIVERSITI MALAYSIA SABAH
2017**

UNIVERSITI MALAYSIA SABAH

BORANG PENGESAHAN STATUS TESIS

JUDUL: **EFFECT OF ELECTRO-CARBURISATION PROCESS ON THE TRIBOLOGICAL BEHAVIOR OF MILD STEEL**

IJAZAH: **DOKTOR FALSAFAH**

Saya **JESTER LING LIH JIE**, Sesi **2012-2018**, mengaku membenarkan tesis Doktor ini disimpan di Perpustakaan Universiti Malaysia Sabah dengan syarat-syarat kegunaan seperti berikut:

1. Tesis ini adalah hak milik Universiti Malaysia Sabah.
2. Perpustakaan Universiti Malaysia Sabah dibenarkan membuat salinan untuk tujuan pengajian sahaja.
3. Perpustakaan dibenarkan membuat salinan tesis ini sebagai bahan pertukaran antara institusi pengajian tinggi.
4. Sila tandakan (/):

SULIT

(Mengandungi maklumat yang berdarjah keselamatan atau kepentingan Malaysia seperti yang termaktub di dalam AKTA RAHSIA 1972)

TERHAD

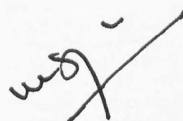
(Mengandungi maklumat TERHAD yang telah ditentukan oleh organisasi/badan di mana penyelidikan dijalankan)

TIDAK TERHAD



JESTER LING LIH JIE
DK1211019T

Disahkan Oleh,
NURULAIN BINTI ISMAIL
PUSAKAWAKILAN
UNIVERSITI MALAYSIA SABAH
(Tandatangan Pustakawan)



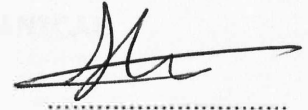
Tarikh: 12 December 2017

(Prof. Madya. Dr. Willey Liew Yun Hsien)
Penyelia

DECLARATION

I hereby declare that the materials in this thesis is my own except for quotations, excerpts, equations, summaries and references, which have been duly acknowledged.

15 July 2017



JESTER LING LIH JIE

DK1221019T



UMS
UNIVERSITI MALAYSIA SABAH

CERTIFICATION

NAME : JESTER LING LIH JIE
MATRIC NO : DK1221019T
TITLE : EFFECT OF ELECTRO-CARBURISATION PROCESS ON
THE TRIBOLOGICAL BEHAVIOR OF MILD STEEL
DEGREE : DOCTOR OF PHILOSOPHY (MECHANICAL
ENGINEERING)
VIVA DATE : 26 OCTOBER 2017

CERTIFIED BY

- SUPERVISOR**
Prof. Madya Dr. Willey Liew Yun Hsien

Signature



UMS
UNIVERSITI MALAYSIA SABAH

A handwritten signature in black ink, appearing to read 'W. L. Hsien', is written over a horizontal line.

ACKNOWLEDGEMENT

I would like to express my sincere gratitude to my supervisor, Assoc. Prof. Dr Willey Liew Yun Hsien for the continuous support of my Ph.D study and research, for his patience, guidance and motivation. Without his guidance and persistent help, this thesis would not have been possible.

I would also like to thank Dr Nancy Julius Siambun for her insightful comments and technical advices. I also thank the fellow staffs and labmates in Fakulti Kejuruteraan (FKJ). They are Mr Jasmi Jaya, Mr Alexander Kong, Mr Saiful Azwar, Mr Saiful Safiq, Mr John Abdullah, Mr Roonie Protasius, and Mr Miron Gakim.

My special thanks to Politeknik Kota Kinabalu, Universiti Teknikal Malaysia Melaka (UTeM) and Universiti Technology Malaysia (UTM) for allowing me to use their instruments for the study. I also wish to thank Ministry of Higher Education (MOHE) for funding the research work (Fundamental Research Grant Scheme FRG0470-2017) and financially supporting me through the programme MyBrain15.

Last but not least, I would like to thank my family: my parents and siblings for moral and emotional support throughout years of study and writing this thesis.

Jester Ling Lih Jie

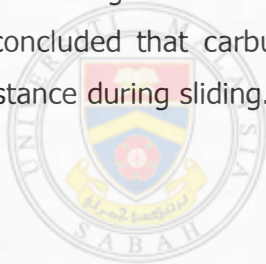
15 July 2017

ABSTRACT

The effect of carburisation process utilizing $\text{Na}_2\text{CO}_3\text{-NaCl}$ as electrolyte on the microstructure and sliding wear behavior of mild steel had been investigated. The carburisation process was conducted at a constant voltage supply of 4.5 V at 860°C for 1 and 3 hours. Sliding tests of the carburised steels were conducted at different loads and speeds under dry, vacuum and oil lubrication conditions. The wear morphology of the sliding tests were analysed. Increasing duration of the carburisation process led to a significant increase in the peak hardness and case depth. The steel specimen carburised for 1 hour had a peak hardness of 910 HV and a case depth of 450 μm . Three hours of carburisation produced higher peak hardness and case depth of 1014 HV and 690 μm , respectively. The hardness were significantly higher than the non-carburised specimen with the hardness of 520 HV. The surface of the carburised specimen was dominated by retained austenite with grain boundaries along with some martensite. Towards the peak hardness, the grain boundaries gradually diminished, and the amount of retained austenite decreased while the amount of martensite increased. In the initial stage of sliding wear test at 10 m/min speed, patches of nascent cavities on the worn surfaces produced by adhesion were formed. These acted as preferential sites for fracture to take place, resulting in a marked increase in the frictional force. Longer carburisation duration also resulted in higher tendency of the carburised layer to form a better anti-wear oxide during sliding. The oxide formed on the worn surface of the specimen carburized for 1 hours was hematite. Both hematite and magnetite known for its better lubricity, were detected on the worn surface of the specimen carburised for 3 hours. The increase in peak hardness and formation of the magnetite enhanced the adhesive wear resistance which in turn reduced the tendency of the specimen to fracture. Longer carburisation duration also resulted in the formation of expanded martensite and shallower grain boundaries with lesser cementite which further enhance the fracture resistance of the carburised specimen. The wear of the counterpart WC ball reflected the severity of fractured worn surface on sliding specimen. At 10 m/min speed, severe fracture caused the formation of severe grooving, cavities, undermined and cracked WC grains.

Whereas, micro-fracture resulted in wear characterised by fine grooves and fewer cavities and undermined WC grains.

Sliding at 70 m/min speed induced formation of magnetite and hematite on the worn surface of specimen carburised for 1 hour. Surface fracturing was hindered when sliding on carburised specimen. The effect of matrix softening was greatly reduced as compared with non-carburised specimens sliding at the same speed. Protrusion was formed on the WC ball sliding on the carburised specimen which replicated from the narrow and deep groove formed on the worn carburised specimen. Under lubricated condition, carburised specimen showed formation of magnetite and hematite on the worn surface at very high load. Cavities was formed owing to the fracture of the oxide on the sliding surface. The oxide debris would either rolled between the gap of the sliding surface, causing reduction in the coefficient of friction or adhered on the mating WC ball that induced groove marks on the worn sliding surface. The results obtained, either in dry or lubrication condition, concluded that carburised 3 hours specimen showed better wear and fatigue resistance during sliding.



UMS
UNIVERSITI MALAYSIA SABAH

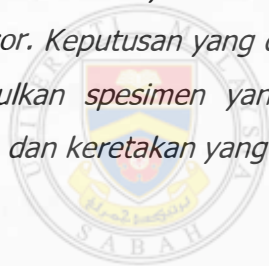
ABSTRAK

KESAN PROCESS ELEKTRO-KARBURISASI PADA KESAN TRIBOLOGI KELULI LEMBUT

Kesan proses pengkarbonan dengan menggunakan $\text{Na}_2\text{CO}_3\text{-NaCl}$ sebagai elektrolit kepada mikrostruktur dan kesan gelongsor haus keluli lembut telah dikaji. Proses pengkarbonan dijalankan di bawah bekalan voltan berterusan 4.5 V pada 860 °C selama 1 dan 3 jam. Ujian gelongsor untuk keluli yang dikarbonkan dijalankan untuk beban dan kelajuan yang berlainan dalam keadaan kering, vakum dan licin. Permukaan haus selepas ujian gelongsor telah dikaji. Tempoh pengkarbonan yang lebih lama meningkatkan kedalaman dan kekerasan puncak. Spesimen yang dikarbonkan selama satu jam mempunyai kekerasan puncak sebanyak 910 HV and kedalaman sebanyak 450 μm . Pengkarbonan selama tiga jam menghasilkan kekerasan puncak sebanyak 1014 HV dan kedalaman sebanyak 690 μm . Kekerasan ini lebih tinggi daripada specimen yang tidak dikarbonkan dengan kekerasan sebanyak 520 HV. Permukaan specimen yang dikarbonkan mempunyai banyak austenit dan sempadan bijirin dengan sedikit martensit. Sempadan bijirin semakin hilang, austenit menjadi kurang, martensit semakin banyak ke arah kekerasan puncak. Di peringkat awal ujian haus gelongsor pada kelajuan 10 m/min, terbentuk kumpulan rongga yang dihasilkan oleh lekatan. Ini bertindak sebagai tempat keutamaan untuk keretakan berlaku, menyebabkan peningkatan yang ketara dalam daya geseran. Proses pengkarbonan yang lebih lama menyebabkan meningkat kecenderungan untuk lapisan dikarbonkan membentuk anti haus oksida. Oksida yang dibentuk atas permukaan haus specimen dikarbonkan selama 1 jam ialah hematit. Kedua-dua hematit dan magnetit kenal dengan lubrisity yang lebih tinggi, dikesan atas permukaan haus specimen dikarbonkan selama 3 jam. Peningkatan dalam puncak kekerasan dan pembentukan magnetit meningkatkan rintangan kehausan pelekat dan mengurangkan kebarangkalian specimen untuk meretak. Tempoh pengkarbon yang lebih lama juga menyebabkan pembentukan martensit berkembang dan sempadan bijirin yang cetek dengan sikit simentit yang meningkatkan rintangan retakan specimen yang dikarbonkan. Retakan teruk dicerminkan oleh kehausan bola pasang WC. Pada kelajuan 10 m/min, retakan teruk disebabkan pembentukan alur teruk, rongga, pelemahan dan peretakan bijirin

WC. Manakala, mikro-retakan menyebabkan kehausan dalam bentuk alur halus, kurang rongga dan pelemahan bijirin WC.

Gelongsor pada kelajuan 70 m/min membentuk hematit dan magnetit di atas permukaan haus spesimen dikarbonkan selama 1 jam. Peretakan di permukaan telah dihalang apabila menggelongsor atas spesimen yang dikarbonkan. Kesan pelembutkan matriks banyak direndahkan berbanding dengan spesimen yang tidak dikarbonkan pada kelajuan yang sama. Penonjolan yang terbentuk di bola WC apabila menggelongsor atas spesimen yang dikarbonkan merupakan replikasi dari alur yang sempit dan dalam atas spesimen haus yang dikarbonkan. Dalam keadaan pelinciran, spesimen yang dikarbonkan membentuk hematit dan magnetit di atas permukaan haus pada beban yang sangat tinggi. Rongga terbentuk disebabkan retakan oksida atas permukaan gelongsor. Serpihan oksida akan menggolek antara celah gelongsor, mengurangkan COF atau melekat di pasangan bola WC dan menyebabkan tanda alur di permukaan haus specimen yang digelongsor. Keputusan yang diperolehi, sama ada dalam keadaan kering atau lincir, menyimpulkan spesimen yang dikarbonkan selama 3 jam menunjuk rintangan kehausan dan keretakan yang lebih tinggi semasa gelongsor.



UMS
UNIVERSITI MALAYSIA SABAH

LIST OF CONTENTS

	Page
TITLE	i
DECLARATION	ii
CERTIFICATION	iii
ACKNOWLEDGEMENT	iv
ABSTRACT	v
<i>ABSTRAK</i>	vii
LIST OF CONTENTS	ix
LIST OF TABLES	xiv
LIST OF FIGURES	xvi
LIST OF ABBREVIATIONS	xlii
LIST OF SYMBOLS	xliv
CHAPTER 1: INTRODUCTION	1
1.1 Background	1
1.2 Problem Statement	2
1.3 Research hypothesis	3
1.4 Research Objectives	3
1.5 Scope of Study	4

1.5.1	Development of Electro-carburisation System	5
1.5.2	Electro-carburisation Process	5
1.5.3	Characterization of Carburised Specimen	6
1.5.4	Tribological Behaviour of Carburised Specimen	6
1.6	Thesis Organisation	6

CHAPTER 2: LITERATURE REVIEW 8

2.1	Introduction	8
2.2	Surface Hardening	8
2.3	Carburisation Process	8
2.4	Carbon Diffusion in Carburisation	14
2.5	Molten Salts Electro-carburisation	17
2.6	Molten Salt Selection	22
2.7	Microstructures of Carburised Steel	23
2.7.1	Ferrite and Pearlite Phase	26
2.7.2	Martensite Phase	27
2.7.3	Bainite Phase	31
2.7.4	Austenite and Retained Austenite Phase	32
2.7.5	Cementite and Carbide Phase	34
2.8	Carburising Case Depth and Hardness	34
2.9	Residual Compressive Stress	36
2.10	Internal oxidation in Carburisation Process	37
2.11	Decarburisation	38
2.12	Wear and Its Mechanisms	39
2.12.1	Adhesive Wear	42
2.12.2	Abrasive Wear	43
2.12.3	Surface Fatigue	46
2.12.4	Erosive Wear	47
2.13	Friction	48
2.14	Effect of Microstructure on Wear	51
2.15	Load and Sliding Speed in Wear	58
2.16	Surface Frictional Heating and Oxidative Wear	61

2.17	Lubrication Effect	66
2.18	Summary	68
CHAPTER 3: METHODOLOGY		70
3.1	Introduction	70
3.2	Material Preparation	71
3.3	Electro-carburisation Process	72
3.4	Specimen Preparation for Hardness Testing	78
3.5	Hardness Testing	78
3.6	Metallographic Analysis	79
3.7	Wear Testing	80
3.8	Lubrication Film Analysis	82
3.9	Surface Profilometer	83
3.10	Characterisation of Carburised Steel Using X-ray Diffractometer (XRD)	84
3.11	Scanning Electron Microscope and Energy Dispersive X-Ray Spectroscopy	87
3.12	Investigation of Oxide Formation using Raman Spectroscopy	88
3.13	Summary	89
CHAPTER 4: EFFECT OF MOLTEN SALT CARBURISATION ON THE HARDNESS AND MICROSTRUCTURE OF MILD STEEL		91
4.1	Introduction	91
4.2	Electro-carburisation Process	91
4.3	Quenching Rate for Different Medium	97
4.4	Hardness and Roughness of Carburised Specimens	98
4.5	Surface Analysis for Carburised Specimens Using SEM	101
4.6	Surface and Subsurface Characterization for Carburised Specimens Using Optical Microscope and EDX	108
4.7	Surface and Subsurface Characterization for Carburised Specimens Using XRD	119

4.8	Estimation of Residual Stress and Strain Based on XRD Results	125
4.9	Summary	128
CHAPTER 5: SLIDING OF CARBURISED SPECIMENS UNDER DIFFERENT DRY SLIDING CONDITIONS		130
5.1	Introduction	130
5.2	Coefficient of Friction in Air and Vacuum at 10 m/min Speed	130
5.3	Coefficient of Friction in Air at 70 m/min Speed	140
5.4	Wear Analysis of the Non-carburised and Carburised Specimens Sliding at Speed of 10 m/min in Air	142
5.5	Wear Analysis of the Non-carburised and Carburised Specimens Sliding at Speed of 10 m/min in Vacuum	164
5.6	Wear Analysis of the Non-carburised and Carburised Specimens Sliding at Speed of 70 m/min in Air	166
5.7	Raman Analysis of the Worn Surfaces of Non-carburised and Carburised Specimens	174
5.8	Wear Analysis on Worn Surface of Carbide Ball	182
5.7	Summary	193
CHAPTER 6: SLIDING OF CARBURISED SPECIMENS UNDER LUBRICATION CONDITIONS		195
6.1	Introduction	195
6.2	Coefficient of Friction under Lubrication Condition	195
6.3	Wear Analysis of Carburised Specimens and Carbide Ball Sliding under Lubrication Conditions	202
6.4	Summary	220
CHAPTER 7: CONCLUSIONS AND RECOMMENDATIONS		221
7.1	Introduction	221
7.2	Conclusions	221
7.3	Contribution	223
7.4	Recommendations	223

REFERENCES

225

LIST OF PUBLICATIONS

243

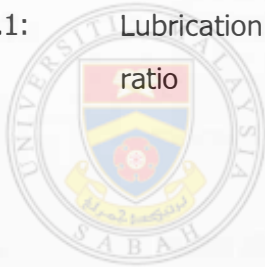


UMS
UNIVERSITI MALAYSIA SABAH

LIST OF TABLES

	Page
Table 2.1:	Characteristics of different carburising process 12
Table 2.2:	Activation energy, Q_d of carbon in iron alloys 16
Table 2.3:	Standard Gibbs free energy changes (ΔG°) and standard potentials (E°) versus $\text{CO}_3^{2-}/\text{CO}_2\text{-O}_2$ for reduction of lithium (Li), sodium (Na) and potassium (K) carbonate to pure metal, carbon, metal oxide and carbon monoxide at different molten salt temperature (MST) 18
Table 2.4:	CO_3^{2-} diffusion coefficient versus the temperature 21
Table 2.5:	Hardness of different phases in steels 24
Table 2.6:	Factors influencing frictional behaviour 49
Table 3.1:	Chemical composition of mild steel shaft received 71
Table 3.2:	Specimen identification for the carburisation process 77
Table 3.3:	Sliding conditions of the pin-on-disc tests 81
Table 4.1:	Surface roughness of molten salt carburised specimens 101
Table 4.2:	Surface roughness for carburised AISI 1020 steel used by Liew <i>et al.</i> (2016) 106

	Page
Table 4.3: EDX elemental analysis of polished C1 and C3 specimens at different polishing interval	115
Table 4.4: EDX elemental analysis of the surface of NC specimen	115
Table 4.5: Retained austenite percentage of carburised specimens	124
Table 5.1: Dominant wear feature observed on the WC ball at 10 m/min speed under 50 and 90 N load	190
Table 5.2: Average wear scar diameter (μm) measured on the WC balls sliding at 10 m/min speed	190
Table 6.1: Lubrication regime estimation based on lambda ratio	202



UMS
 UNIVERSITI MALAYSIA SABAH

LIST OF FIGURES

	Page	
Figure 1.1:	Research process flow chart.	5
Figure 2.1:	Iron-carbon equilibrium phase diagram.	10
Figure 2.2:	(a) Body-centered cubic (BCC) ferritic and (b) face centered cubic (FCC) structures.	11
Figure 2.3:	Fick's second law for diffusion of carbon into a material, C_s : constant surface concentration of the diffusing species, C_0 : initial bulk concentration and a constant diffusion coefficient, D .	15
Figure 2.4:	Potential versus temperature trends with region of carbon and carbon monoxide production in molten Li_2CO_3 , Na_2CO_3 and K_2CO_3 salt mixture.	19
Figure 2.5:	Phase diagram of Na_2CO_3 and NaCl salt mixtures with increasing mole of Na_2CO_3 .	23
Figure 2.6:	Effect of carbon on hardness of (a) various microstructures in steel and (b) martensitic (M) and austenitic (A) steel.	25
Figure 2.7:	Continuous cooling transformation (CCT) diagram in steel (line (a): slow cooling, line (b): normal cooling, line (c): rapid cooling).	26
Figure 2.8:	SEM micrograph of pearlitel with fine interlamellar spacing at 10000X magnification.	27

	Page
Figure 2.9:	Schematic representation of tetragonal martensite with iron atom displaced by carbon atom (black circles). 28
Figure 2.10:	Schematic morphology of (a) lath and (b) plate martensite. 28
Figure 2.11:	Microstructure of (a) lath and (b) plate martensite at 200X and 1000X magnification respectively. 29
Figure 2.12:	Unit cell dimension for carbon (open circles and full line) and nitrogen (full circles) martensite. 29
Figure 2.13:	Effect of carbon content on martensite start (M_s) temperature and volume percent (PCT) of retained austenite in as-quenched martensite. 31
Figure 2.14:	TEM micrograph of (a) upper and (b) lower bainitic steels. 32
Figure 2.15:	Carburised case microstructure containing (a) 8 % and (b) 30 % of retained austenite. 33
Figure 2.16:	Hardness as a function of steel carbon content. 36
Figure 2.17:	Oxidation potential of alloying elements and iron in steel. 37
Figure 2.18:	Equilibrium pressure of CO and CO ₂ for $2\text{CO} \rightarrow \text{CO}_2 + \text{C}$ reaction. 39

	Page	
Figure 2.19:	Wear mapping of medium carbon steel with thick line represent different wear mechanisms, thin line are contours of equal wear rates and chain line represent constant value of the pV factor.	41
Figure 2.20:	Classification of mechanical wear processes.	42
Figure 2.21:	Illustration of adhesive wear. Arrow: sliding direction, v : sliding velocity.	43
Figure 2.22:	Illustration of (a) two and (b) three body abrasion system. Arrow: sliding direction, v : sliding velocity.	44
Figure 2.23:	Possible mechanisms for particles during sliding: (a) rotation, (b) skidding, (c) rolling, (d) entrapment.	44
Figure 2.24:	Schematic representation of wear loss by hard particles as a function of hardness of abrasive particle.	45
Figure 2.25:	Effect of grain size (d) on (a) two body, (b) three body abrasive wear (critical grain size: d_c , transition grain size: d_t).	46
Figure 2.26:	Process of wear particles formation at the subsurface.	47

		Page
Figure 2.27:	Location of maximum tensile stress and shear stress.	48
Figure 2.28:	Schematic of the energy flows in a system sliding with velocity (v) and normal force (F_n). The total dissipated power (\dot{E}_{tot}) is the integral of energy dissipated by heat (\dot{E}_q), wear (\dot{E}_w) and entropy change of material (\dot{E}_m).	50
Figure 2.29:	Correlation between abrasive wear resistance of steel with carbon content.	54
Figure 2.30:	Schematic of the cross sectional view of plastically deformed worn surface. ϵ indicated the equivalent plastic strain that caused delamination wear.	55
Figure 2.31:	Schematic of abrasive wear resistance of different materials as a function of their bulk hardness. Orange region: martensite, yellow region: martensite and retained austenite.	57
Figure 2.32:	Effect of metal hardness, abrasive hardness and presence of hard phases on the abrasion wear resistance.	58
Figure 2.33:	Effect of carbides on the wear resistance of steel.	58
Figure 2.34:	Wear map for 0.2% C steel under dry sliding. The wear rates were showed by the straight line inside the map in the power of 10^{-6} .	59

		Page
Figure 2.35:	Model of a contact between a typical dominant plateau on the surface of the pin and a typical contact on the disc: (a) oxidized plateau during sliding, (b) instantaneous N circular asperity contacts of diameter $2a$ ($a \approx 1 \mu\text{m}$), (c) fully oxidized plateau about to shear at a critical oxide thickness (T_c : contact temperature, T_s : sliding temperature, ξ : critical oxide thickness).	61
Figure 2.36:	Schematic representation of oxidational wear: (a) oxide films growth on asperity contacts, (b) break off of critical oxide film as wear debris, (c) repetition of new oxide growth and breaks off (F : normal force, v : sliding velocity, $2a_0$: asperity contact area).	63
Figure 2.37:	Schematic of compacted oxide layers from wear debris particles: (a) material transfer of metallic wear, (b) comminution, oxidation and agglomeration of debris particles, (c) compaction of agglomerated debris particles, (d) development of "glaze" layer over compacted particle layer, (e) breakdown and development of new wear protective layer.	64
Figure 2.38:	Critical hardness levels with carbon content.	65
Figure 2.39:	Stribeck curve with different lubrication regimes (μ : viscosity, U : speed, F : load).	67
Figure 2.40:	Wave-like topography of a lubricated worn surface.	68

	Page	
Figure 3.1:	Flow diagram of the overall experimental procedure.	71
Figure 3.2:	Equipment set up for the carburisation process.	73
Figure 3.3:	Customized (a) cylindrical retort and (b) square lid.	74
Figure 3.4:	Assembly of the equipment used for carburisation process.	75
Figure 3.5:	Arrangement of mild steel specimen for carburisation process.	76
Figure 3.6:	Illustration of the diamond indenter.	78
Figure 3.7:	Schematic of ball on disc wear test system (F = normal force on the pin, d = pin or ball diameter, D = disc diameter, R = wear track radius, w = rotation velocity of the disc).	81
Figure 3.8:	Accountable wear volume loss (dark region) in a wear trace.	84
Figure 3.9:	Diffraction of x-rays by a crystal.	85
Figure 3.10:	Example of Williamson-Hall plot.	87
Figure 3.11:	Raman spectra at different laser power spotted on the worn surface of carburised specimen (M: Magnetite, H: Hematite).	89

	Page	
Figure 4.1:	Picture of mild steel specimens produced (a) with electrolysis and (b) without electrolysis.	92
Figure 4.2:	Raman spectra for unelectrolysed specimen (M: Magnetite).	92
Figure 4.3:	Optical micrographs of the perpendicular cross section of the specimen produced (a, c) without and (b, d) with electrolysis for 1 hour and water quenched. (a) and (b) is the subsurface just below the surface. (c) and (d) is the core.	94
Figure 4.4:	The microstructure at (a) 5 μm and (b) 15 μm beneath the surface parallel to the flat surface of water quenched unelectrolysed steel. (a) At the subsurface of 5 μm beneath the surface, no visible microstructure appeared. (b) At the subsurface 15 μm beneath the surface, mixed microstructure appeared.	95
Figure 4.5:	Current profile for carburisation duration of (a) 1 hour and (b) 3 hours under 4.5V. Solid line indicated high amount of chemical reactions occurred during the electrolysis process. Dashed line indicated reduction of chemical reactions during electrolysis process.	97
Figure 4.6:	Quenching rate for different quenching medium.	98
Figure 4.7:	Variation of the subsurface hardness of carburised and non-carburised specimens.	99

	Page
Figure 4.8: Nital etched cross section of (a) C1, (b) C3 and (c) OC1 specimens.	100
Figure 4.9: SEM examination of the unworn surface of C1 specimen at (a) lower magnification and (b) higher magnification that showed numerous amount of carbon rich elements at the grain boundaries.	102
Figure 4.10: SEM examination of the unworn surface of C3 specimen at (a) lower magnification and (b) higher magnification that showed the grain boundaries serration/waviness within the grain.	102
Figure 4.11: Surface profile of the (a) C1 and (b) C3 specimens.	104
Figure 4.12: SEM images of the surfaces of specimen carburised for (a-b) 1 and (c-d) 3 hours. Specimen carburised for 1 hour had grains with a diameter of 10-20 μm . Specimen carburised for 3 hours had larger grains with a diameter of 10-150 μm and higher amount cementite precipitates in the grain boundaries.	105
Figure 4.13: Surface profile of the specimen carburised for (a) 1 and (b) 3 hours and water quenched as reported by Liew <i>et al.</i> (2016).	106